Mechanical & Interfacial Properties of Bamboo Lamella-PP Composites – Effect of Lamella Treatment

Pierre Ovlaque, Marie Bayart, Patrice Cousin, Julien Durand, Grégoire Mercusot, Saïd Elkoun, and Mathieu Robert*

Center for Innovation in Technological Ecodesign, University of Sherbrooke, Sherbrooke, Quebec J1K 2R1, Canada

Abstract: This study aims at measuring the interfacial properties of natural fibers in polypropylene composites by the mean of direct methods of characterization. Bamboo lamellae (BL) and polypropylene (PP) were used to produce laminated composites with continuous and homogenous interfaces. This research also focuses on the effect of maleic anhydride-grafted PP (MAPP) on the improvement of the PP/BL composites interfacial properties, which were measured by the means of the double cantilever beam (DCB), end-notched flexure (ENF) and short beam shear (SBS) methods. Flexural properties of the different composites were also determined using the three-point bending and single cantilever modes by dynamic mechanical analysis (DMA). The retention rates (Rr) of mechanical and interfacial properties were calculated on samples aged in hot water. Results reveal that MAPP induced a significant increase in flexural properties. This is undeniably related to an enhancement of affinity between PP and BL that was confirmed by DCB, ENF and SBS tests results. It was also highlighted that MAPP tends to limit degradation of the composite interfacial properties with,for instance, a critical fracture toughness (mode I) Rr of 97 % for MAPP coated composites against 56 % for the untreated composites.

Keywords: Polypropylene, Bamboo, Double cantilever beam, End-notch flexure, Short beam shear

Introduction

The use of natural fibers (NF) as a replacement for synthetic reinforcements has been expanding in the automotive industry for the last decades due to political pressure and weight-saving necessities [1-3]. Thus, it is usual to find polypropylene (PP) or polyethylene reinforced with flax, kenaf or even jute in car interiors nowadays [2,4]. However, despite a lower environmental impact and price [5], NF reinforced polymers (NFRP) are not perfectly suited for the automotive industry. Their moisture instability and interface incompatibility are difficult to manage and limit their use in structural and outdoor applications [1,6]. Those limitations are mainly related to weak interfaces that indorse voids and delamination which lead to premature failure of NFRP [6-8]. In addition, weak interfaces lead to greater water absorptions and therefore to swelling of NF, which generate cracks in NFRP [9,10].

It has been well known for decades that the main reason for those problematic weak interfaces between NF and non-polar polymeric matrices is the hydrophilic nature of NF [11-13]. Thus, it is well established in the literature that surface treatments can successfully enhance the affinity between matrices and NF and help to improve NFRP properties. Several chemical treatments have been proposed to compatibilize NF with polymer matrices such as alkali treatments or silanization [14-18]. Still, maleic anhydride grafted PP (MAPP) is very effective for NFRP mechanical properties enhancement [12,19,20]. Improvements of PP/jute composites flexural strength of 72 % and 15 % were

reported by Mohanty *et al.* and Hong *et al.* respectively, thanks to MAPP [21,22].

However, due to the difficulty of producing composites with appropriate homogeneous interfaces, it is hard to quantify the improvement of the interface after the processing steps. On the one hand, randomly dispersed fiber composites do not permit direct measurement of interfacial properties due to the lack of continuity of the interface. On the other hand, for laminated NFRP produced with fabrics and mats, the matrix penetrates inside the fabric layer (i.e., bridging between layers), which leads to the absence of well-defined continuous interfaces in the composites. Consequently, the interfacial properties of the NFRP are often extrapolated from indirect methods such as mechanical testing and fractography.

In order to measure the improvement of the interface related to surface treatments, bamboo lamellae (BL)-based composites were produced. The use of BL has the advantage of creating composites exhibiting well-defined continuous interfaces and no bridging between layers. Therefore, BL-based composites can be used for characterization methods dedicated to the interface adhesion characterization such as ASTM D5528 and D7905/D7905M (i.e., mode I and mode II interlaminar fracture toughness of unidirectional fiber-reinforced polymer matrix composites respectively). Eventually, the data obtained with BL composites could be extrapolated to other types of composites such as short fiber composites.

The objective of the present work is to quantify the efficiency of MAPP enhancement in a model compound produced by thermocompression (i.e., BL and PP laminated composites). A MAPP coating was applied on lamellae to enhance their adhesion to PP. Several characterizations were

---
*Corresponding author: Mathieu.Robert2@USherbrooke.ca

performed to focus on composites interfacial properties toughness in mode I and mode II fracture opening (i.e., tensile stress normal to the interface and shear stress parallel to the interface respectively). Mechanical and thermomechanical tests were carried out as well as aging of the composites to study the interfacial degradation.

Experimental

Material

Bamboo lamellae were purchased from Cobratex, France and used in their original lamella shape (width=10 mm, thickness=400 μm). A non-ionic maleated polypropylene (MAPP) emulsion graciously provided by Michelman (reference ME91735) was used for coating. Highly crystalline polypropylene (F006EC2 homopolymer PP; Tg=8 ^{o}C and Tm=164 ^{o}C) was provided by Braskem.

Bamboo Lamella Treatment and Composites Processing
Coating

Raw bamboo lamellae (BL) were immersed in the MAPP emulsion for 10 seconds. The excess of emulsion was removed from the surface. Coated BL (MAPP-BL) were then dried for 24 h at room temperature. BL masses before immersion and after drying were used to control the coating deposition. A mass increase of 13 % was attributed to the coating.

Composites Processing

Two different composites made of PP sheets (thickness 300 μm) and BL or MAPP-BL (thickness 400 μm), namely PP-BL or PP-MAPP-BL respectively, were prepared by alternately stacking 5 layers of PP and 4 layers BL or MAPP-BL. The material was then hot pressed at 200 ^{o}C using a Carver hydraulic press. The processing was performed according to the following cycle: 5 min without compressive stress (i.e. 0 ton (T)), 1 min at 3T, 1 min at 4T and 1 min at 5T (force applied on 100 cm^2). 30 sec releases were performed between each step in order to relieve the pressure and avoid the presence of air bubbles in composites. Finally, composites were cooled down at 20 ^{o}C/ min to room temperature. The resulting composite size was 10×130×3 mm.

Methods
Water Absorption Study and Conditioning

Water absorption was performed according to ASTM D570. Neat resin and composite samples were dried at 50 ^{o}C until a constant mass was obtained and then immersed in 50 ^{o}C water. Water absorption was calculated following equation (1):

$$W(\%) = \frac{M_t - M_0}{M_0} \times 100 \tag{1}$$

where M_0 is the mass of the dry sample and M_t the mass after immersion during a given time. The test was stopped when saturation was achieved.

Mechanical Properties

BL tensile tests were performed on raw and coated BL following ASTM D3039 using a Zwick/Roell z050 machine equipped with a 30 kN load cell. The Young's modulus (E), ultimate tensile strength (UTS) and elongation at break (ε) were determined using a span of 30 mm and a speed of 2 mm/min on more than 25 specimens per type of sample.

Flexural tests were performed according to ASTM D790 with a span-to-thickness ratio set at 16:1 and the crosshead speed at 1 mm/min. The average flexural modulus (E_f) and ultimate flexural strength (UFS) were determined on more than five specimens per condition.

Dynamic mechanical analysis (DMA) was carried out on a Perkin Elmer DMA 8000. Single cantilever scans were carried out from -75 to 150 ^{o}C with a frequency of 1 Hz, a 1 N static force and a strain of 0.05. The storage modulus and tangent δ of the different conditions were determined at 25 ^{o} and 100 ^{o}C on more than five samples per conditions in order to monitor the effect of the temperature on the composite interface.

Interfacial and Fracture Toughness Properties

The toughness of the interface was tested using the modes I and II fracture opening as illustrated in Figure 1 to obtain a direct assessment of interfacial improvement. Double cantilever beam (DCB), end-notched flexure (ENF) and short beam shear (SBS) tests are three methods used to characterize the interfacial adhesion of composites, particularly when they are laminated. DCB induces tensile stress at the matrix/fiber interface as described by the mode I fracture opening. Conversely, ENF and SBS loading induce intense shear stress at the fiber/matrix interface that corresponds to a mode II solicitation. Neat PP was not tested under mode I and mode II fracture opening due to the absence of interface in its bulk.
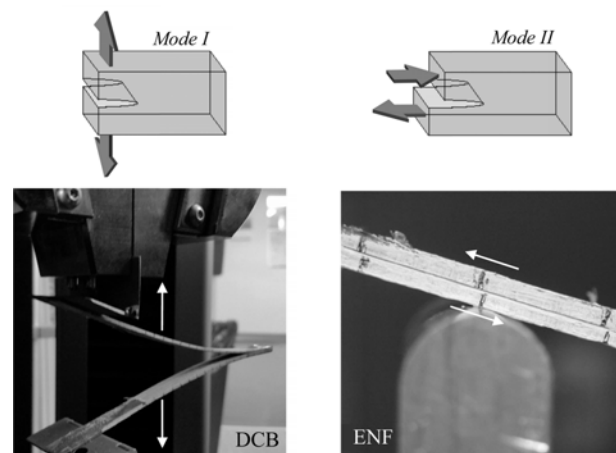

Figure 1. Mode I and II of fracture opening and DCB and ENF assemblies.

Figure 2. Sample for interlaminar fracture toughness modes I and II.

Short beam shear tests were carried out on composite materials according to ASTM D2344 standard to determine their maximal interlaminar shear strength (ILSS). The span-to-thickness ratio was set at 4:1 and the crosshead speed at 1 mm/min. More than five specimens per type of sample were tested. The ILSS was calculated according to equation (2):

$$ILSS = \frac{3}{4}\frac{P_m}{bd} \tag{2}$$

where P_m is the maximal applied load, and b and d the width and the thickness of the specimens, respectively.

Critical interlaminar fracture toughness (mode I) (G_{IC}) tests were carried out following ASTM D5528 using double cantilever beam loading (DCB). 3 mm thick composites with a 30 μm thick PTFE inserts were specially produced for DCB tests as shown in Figure 2. Piano hinges assembly was chosen and hinges were glued to the inserts edge of composites using a cyanoacrylate-based glue. The initial loading and reloading phase speeds were set at 1 mm/min and the unloading phase speed at 20 mm/min. Live crack propagation in the sample was recorded using a Motic camera (moticam 580) mounted with a 12 mm lens to ensure a sufficient magnification of the delamination process. The initial loading phase was stopped after a delamination length of 5 mm. G_{IC} was calculated out of 5 specimens for each increment of 5 mm of the delamination until a length of 85 mm from the load point in the reloading phase was reached. The modified beam theory method was used to calculate G_{IC} following equation (3):

$$G_{IC} = \frac{3P\delta}{2b(a+|\Delta|)} \times F \tag{3}$$

where P is the applied load, δ the load point deflection, b the width of the specimen, a the delamination length and Δ the effective delamination extension. A large displacement factor correction (F) was applied when the ratio of δ to a was greater than 0.4. F was calculated according to equation (4):

$$F = \left(1 - \frac{3\delta^2}{10a^2} - \frac{3\delta t}{2a^2}\right) \tag{4}$$

where t is the distance between the hinge rotation axis and the insert. F was set equal to 1 for ratios of δ lower than 0.4.

Critical interlaminar fracture toughness (mode II) (G_{IIC}) was performed according to ASTM D7905/7905M on non-pre-cracked specimens. End-notched flexure samples were produced as described in Figure 2 and the notch length (i.e., the PTFE insert length) was set at 45 mm. Flexural tests were performed at a speed of 0.5 mm/min for both

compliance calibrations and fracture tests. The non-pre-cracked toughness was calculated following equation (5).

$$G_{IIC} = \frac{3P_{max}^2 a_0^2 m}{2B} \tag{5}$$

where P is the applied load, a_0 the delamination at start position, B the width of the specimen and m the compliance calibration coefficient.

All tensile, flexural, modes I and II interlaminar fracture toughness and SBS tests were performed on a Zwick/Roell z050 testing machine equipped with a 30 kN load cell.

Lamella and Composite Morphology

Optical microscopy (OM) images were acquired with a Nikon Optiphot combined to a Motic moticam 580 digital camera and the Motic Plus 3.0 software to determine the microscale morphology of BL as well as the fracture location after DCB tests.

Scanning electron microscope (SEM) was performed on a Hitachi S3000-N at 5 kV on metalized samples to determine the structure of bamboo lamella and characterize the thickness of the coating.

Statistical Analysis

A calculation of the T-scores was carried out to verify the reliability of the quantitative data obtained for the different samples and conditions. This was done according to equation (6):

$$T\text{-}score = \frac{A_i - A_j}{\sqrt{\frac{\sigma_i^2}{n_i} + \frac{\sigma_j^2}{n_j}}} \tag{6}$$

where A_i and A_j are the mean values of the characteristic measured for samples i and j. σ_i and σ_j are the standard deviations found for these same samples and n_i and n_j the number of specimens tested for each condition.

A confidence interval of 95 % was considered as long as the P-value was below 0.05.

Results and Discussion

Lamellae Characterization and Effect of the Coating

BL Geometry and Morphology

An OM cross-section of a BL is presented in Figure 3(a) and revealed a very heterogeneous assembly composed of two distinct structures. On the one hand, bamboo cellulosic fiber bundles appeared in a dark-gray color under reflective light mode. SEM magnification of this area highlighted a dense assembly of hexagonal cellulosic fibers that are responsible for the good mechanical properties of bamboo culms. On the other hand, the continuous phase that appeared in white color under OM corresponds to the parenchyma tissue [23]. SEM magnification of parenchyma tissue exhibits a highly porous structure which maintains the fiber strands aligned along the bamboo culm axis [24].
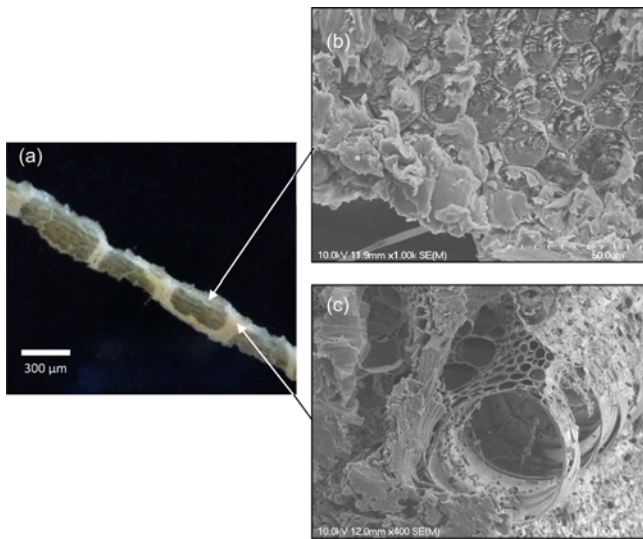
Figure 3. OM picture of a bamboo lamella (transversal cut) (a) and SEM pictures of a bamboo fiber strand (b) and bamboo parenchyma tissue (c).

Concerning the surface of BL, Figure 4 shows a fiber strand with a rough surface that could help the mechanical interlocking with PP. Conversely, the MAPP coating gives a smoother surface with drying shrinkage cracks. As suggested by Figure 4(c), the thickness of the MAPP coating varies between 15 and 25 μm. The cracks are not a problem since the MAPP coating will melt in BL surface vicinity during the processing and should improve the mechanical properties [12,21].
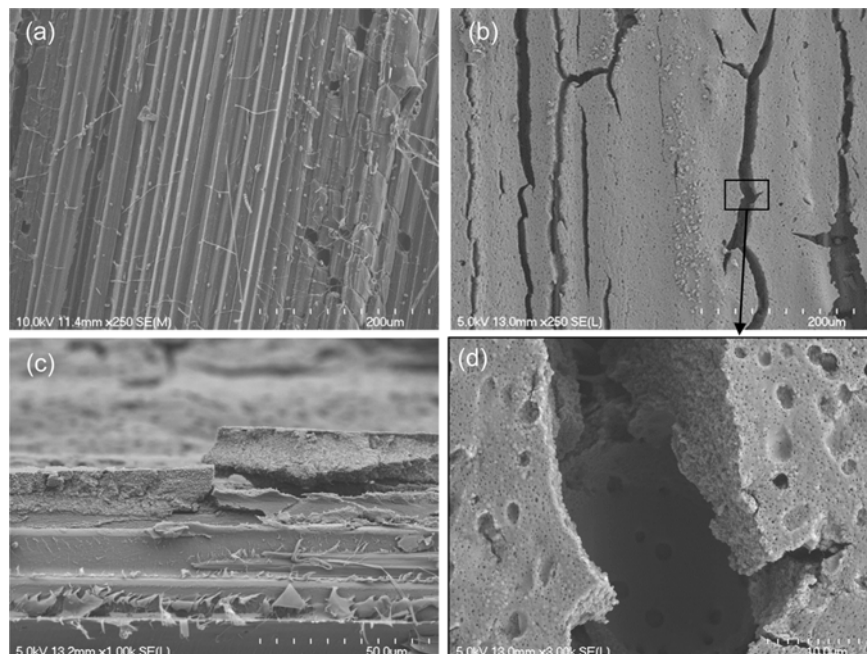
Table 1. Tensile mechanical properties of BL and coated BL (MAPP-BL)

	E (GPa)	SD	UTS (MPa)	SD	ε (%)	SD
BL	16.2	5.5	202	62	1.46	0.27
MAPP-BL	16.5	3.3	160	51	1.08	0.34

Mechanical Properties

Tensile properties of BL and MAPP-BL are presented in Table 1. It is noteworthy that the standard deviation of the Young's modulus (E), ultimate tensile strength (UTS) and elongation at UTS (ε) are substantial due to the high heterogeneity of BL. Hence, it can be noticed that the application of the coating does not alter the mechanical properties of the material. The slight decrease of the UTS could be attributed to the increase of the cross-section of the samples induced by the coating.

Matrix and Composites Properties
Flexural Properties

The flexural properties calculated on PP, PP-BL and PP-MAPP-BL composites are presented in Figure 5. PP exhibits a flexural modulus of 1.31 GPa and a UFS of 49.2 MPa that corresponds to standard values for PP matrices. The addition of 50 % in volume of BL to the PP matrix induces a drastic increase of 336 % and 99 % of E_f and UFS, respectively. This improvement is mainly attributed to the good mechanical properties of the cellulosic fiber bundles in BL [25]. Indeed, cellulosic fibers are well known for their high tensile properties, which have played the role of
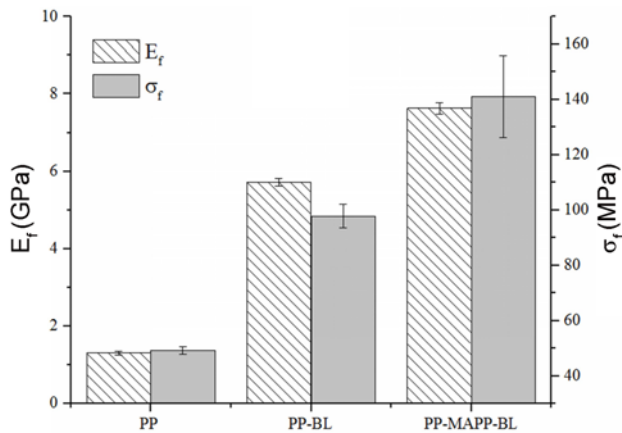

Figure 4. SEM micrographs of BL (a) and MAPP-BL (b, c, and d) surface.

Figure 5. Flexural modulus (E_f) and UFS (σ_f) of PP, PP-BL and PP-MAPP-BL (standard deviation (SD) as error bars).

reinforcement in the lower part of the sample (i.e., beam in traction). In the upper part (beam in compression), the strand configuration and parenchyma tissues limit the wear down of the fibers and induce a strengthening [24]. Despite the strong improvements induced by the additions of BL in PP matrix, PP-MAPP-BL composites results demonstrate that the stress transfer between the resin and the lamellae is not naturally optimal. Indeed, the comparison between PP-BL and PP-MAPP-BL composites gives a flexural modulus increase of 33 %, from 5.7 to 7.6 GPa. Moreover, the UFS rises from 98 MPa for PP-BL to 141 MPa for PP-MAPP-BL,

which corresponds to a 44 % increase. The enhancement of the composites flexural properties is clearly related to the addition of MAPP and the formation of covalent bonding at the interface between the two components.

Thermomechanical Properties

In order to assess the impact of temperature, mechanical properties at 25 and 100 °C, which correspond to the end of the β and α relaxation of PP respectively, were compared using DMA results presented in Figure 6.

Both PP relaxations present a different origin. On the one hand, β-relaxation, which can be spotted around 8 °C in both tangent δ and storage modulus plots, is related to the glass transition temperature (Tg) of the amorphous phase [26,27]. On the other hand, α-relaxation is related to the rigid amorphous fraction, also known as RAF, trapped in the crystalline system [26,27]. No significant modification of Tg nor Tα were measured between PP, PP-BL and PP-MAPP-BL as PP chain movement is only limited in the vicinity of BL and, thus, most of the PP chains are not restricted by BL. However, β- and α-relaxation in neat PP appear to be more intense compared to that of both composites. It is more than likely that the elastic behavior of BL, which accounts for 50 % of the volume of the composite, minimized the viscoelastic relaxation measured by DMA and lowered the effect of both transitions. This is even more remarkable at 75 °C (i.e. α-relaxation) because the differences between the elastic behavior of BL and the viscoelastic behavior of PP are more pronounced.
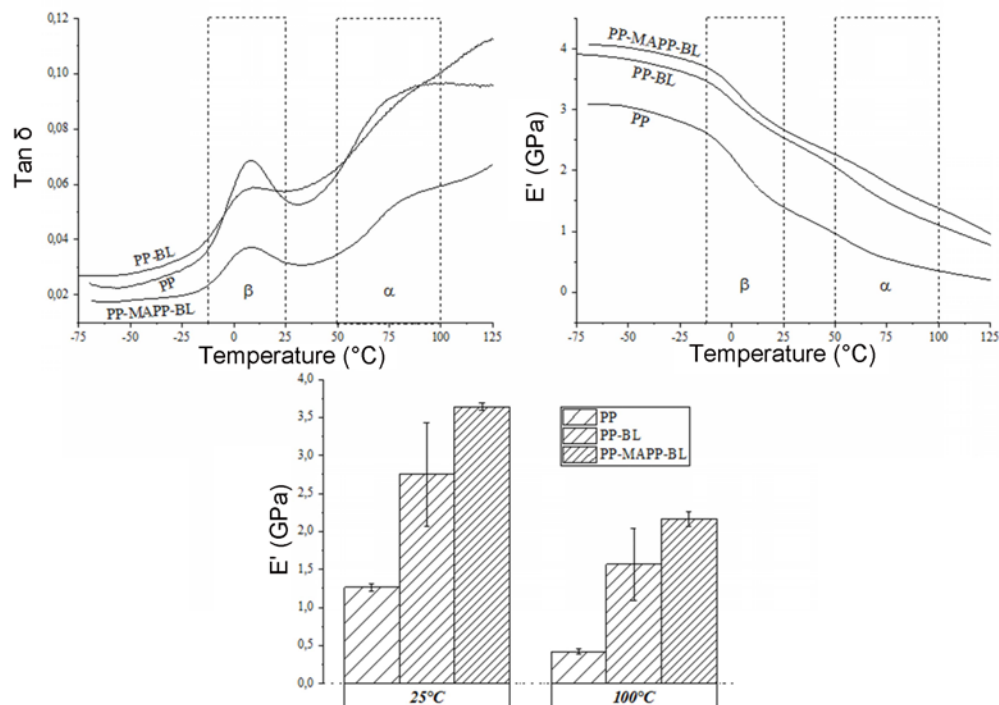
Average values and standard deviations of storage

Figure 6. DMA results of PP, PP-BL and PP-MAPP-BL; (a) tan δ, (b, c) storage modulus E'.

modulus after the ending of β-relaxation (25 $^{\circ}$C) and α-relaxation (100 $^{\circ}$C) are presented in Figure 6(c). Composites exhibit a dramatic increase in their storage modulus compared to neat PP that was attributed to BL. It is noteworthy that the effect of MAPP coating can be noticed as an improvement of 32 % was measured on average values between PP-MAPP-BL and PP-BL. Moreover, this enhancement is maintained after the second relaxation (37 %). However, the MAPP coating does not limit property decrease at high temperature. Decreases of 67 %, 43 % and 41 % were measured from 25 to 100 $^{\circ}$C for PP, PP-BL and PP-MAPP-BL respectively. The limited decrease of storage modulus found for both composites compared to PP was attributed to BL that do not demonstrate high loss of properties from 25 to 100 $^{\circ}$C.

Interfacial Properties

Mode I interlaminar fracture toughness (G_{IC}) values calculated from the DCB test are presented in Figure 7. It is noteworthy that both composites interfaces seem homogenous along their length, as G_{IC} stays steady while the crack length increases.

However, results of G_{IC} should be considered with the micrograph of the crack area (Figure 9). Considering only the results of the DCB test, it could be easy to conclude that the coating does not induce a strong improvement of G_{IC} for PP-MAPP-BL composites. Nonetheless, a major difference was noticed between both conditions regarding the location of the crack propagation. In PP-BL, crack propagation take place at the PP/BL interface as demonstrated in Figure 7(b) while for PP-MAPP-BL, crack propagation occurs inside BL as demonstrated in Figure 7(c). Hence, it is possible to conclude that the MAPP coating has successfully improved the G_{IC} values of the interface as the crack propagation is shifted to a weaker area (i.e., the inner cohesion of BL). According to averages values of G_{IC}, it appears that BL exhibit an inner interlaminar fracture toughness of 196± 23 MPa whereas the natural interlaminar fracture toughness of the PP/BL interface is 171±17 MPa. Therefore, it is not possible to measure the interlaminar fracture toughness of the PP/MAPP/BL interface due to the displacement of the crack location.

The low G_{IC} of BL (i.e., 196 MPa) in PP-MAPP-BL DCB tests can be explained by the fact that wood and bamboo exhibits lower mechanical properties in the transversal direction of the cellulosic fiber axis [28,29]. It has been proved that the strong cellulose fibers do not participate in transversal properties due to their particular structure [30]. In addition, the easy delamination of bamboo in the DCB tests can also be explained by the absence of natural selection of bamboo based on this criterion. Indeed, bamboo exhibits very short branches along its culm and is therefore not naturally tailored to withstand a mode I opening which is not a selective advantage among the bamboo population. Conversely, mode II opening resistance appears to be a selective advantage as bamboo culm need to resist wind solicitation and therefore intense shear in the culm.

DCB test proves that surface treatments are a quite limited solution to improve the G_{IC} of a composite made of BL. The G_{IC} of the interface between PP and BL is in fact only 25 MPa lower than that of BL, which represents an impassable limit that cannot be improved (i.e., the weakest constituent among PP, BL and the interface).
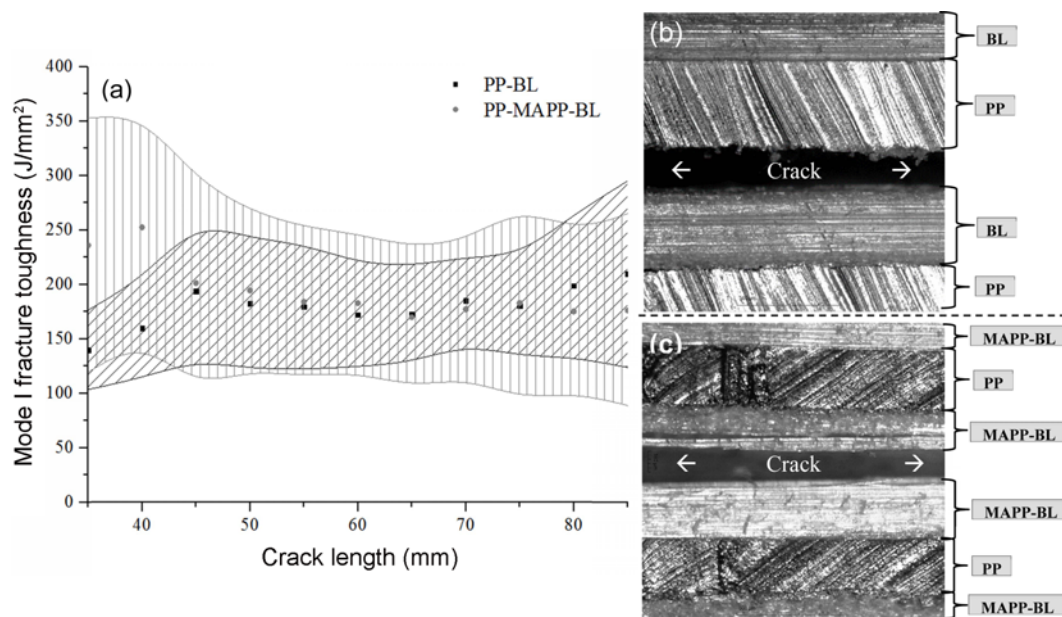

Figure 7. (a) Mode I interlaminar fracture toughness as a function of crack length (SD as area), (b) micrograph of the rupture area at the interface in PP-BL composite, and (c) micrograph of the rupture in the bamboo lamella in PP-MAPP-BL composite.
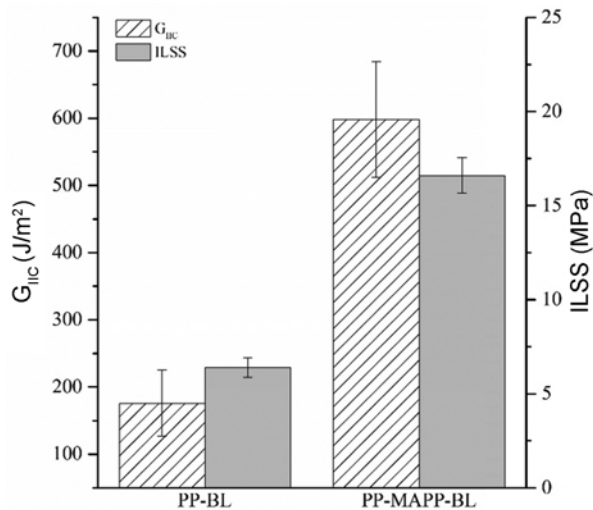
Figure 8. PP-BL and PP-MAPP-BL G_{IIC} and ILSS results (SD used for error bars).

ENF and SBS results are presented in Figure 8. The critical interlaminar fracture toughness in mode II (G_{IIc}) calculated via ENF tests reveals a drastic improvement of PP-MAPP-BL toughness. An increase of 240 % was calculated between the critical toughness of PP-BL and PP-MAPP-BL. These results demonstrate a great enhancement of the fiber/matrix interfacial adhesion thanks to the MAPP coating. This result is confirmed by SBS tests, which show a 160 % increase of the ILSS with the MAPP-treated bamboo. It is clear from the results that, unlike G_{IC}, G_{IIC} and the ILSS

can be successfully enhanced by a surface treatment as the G_{IIC} and ILSS of PP and BL are naturally very high.

The improvement of the interface is supported by the SEM micrographs presented in Figure 9. Due to the differences of polarity and hydrophilicity, PP and BL do not present a natural affinity that limits the load transfer. In contrast, the affinity between PP and BL was greatly improved by the MAPP coating, which explained the improvement of mechanical and interfacial properties observed above.

Ageing

PP, PP-BL and PP-MAPP-BL were immersed in 50 °C water in order to perform accelerated ageing. Saturation of water uptake calculated according to equation (1) was reached after 300 hrs and ageing was stopped after 400 hrs. Samples were then oven dried at 50 °C to remove water that could impact the mechanical tests. Samples were allowed to equilibrate with the environment of the laboratory for 24 hours (i.e., temperature and humidity) before any further analysis/testing.

Components Degradation

Both components used for composite processing (i.e., BL and PP) were aged in water separately in order to isolate the interfacial degradation from the degradation of the components. As demonstrated in Table 2, neither BL nor PP exhibits a strong decrease in their mechanical properties as retention rates (Rr) of PP and BL are ranging around 100 %. Only the storage modulus of PP seems to decrease at 100 °C after ageing (Rr=89 %). Regarding BL, no significant modification of BL properties was measured due to high standard
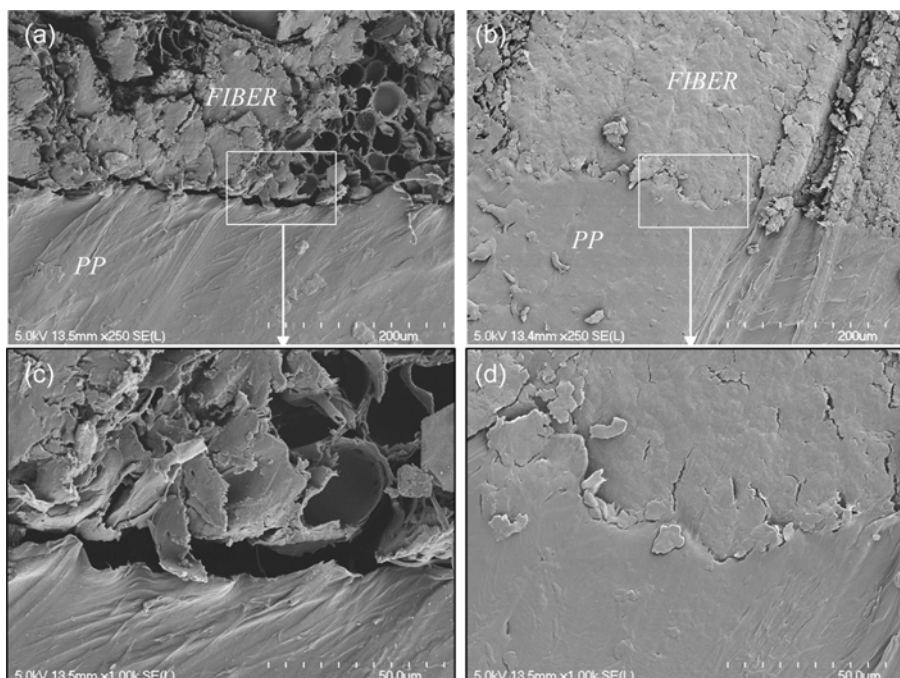

Figure 9. SEM micrographs of the interface between PP and BL; (a) and (c) without MAPP treatment, (b) and (d) with MAPP treatment.

Table 2. Mechanical properties and Rr of PP and BL after a 400 h ageing in water

In MPa	PP		Rr
	Unaged	Aged	
E (20 $^{\circ}$C)	1160±125	1130±92	97 %
UFS (20 $^{\circ}$C)	49.2±1.3	48±1.2	98 %
E' (25°C)	1265±51	1184±91	94 %
E' (100°C)	420±35	373±35	89 %

In MPa	BL		Rr
	Unaged	Aged	
E (20 $^{\circ}$C)	15.1±4.18	18.5±4.44	123 %
UTS (20 $^{\circ}$C)	192±59.3	201±49.7	105 %

deviations found for E and UTS values. Consequently, any degradation of composite properties after ageing can be mostly related to interfacial degradation.

Composites Properties

Mechanical properties determined via three-point bending flexural testing and DMA before and after ageing are presented in Table 3. It is noteworthy that the data tend to reach the same values of residual properties (Rr). The lower Rr calculated for the storage modulus at 100 $^{\circ}$C could be related to the higher degradation of PP properties at 100 $^{\circ}$C as discussed above. PP-MAPP-BL composite presents better residual properties than PP-BL composite, which shows the protective effect of the MAPP coating on the ageing in water.

Table 4 reports the residual bonding properties at the interface. Ageing in water induces a noticeable decrease in the values of ILSS, G_{IIC} and G_{IC} in both composites. Rr of ILSS are perfectly in line with that of mechanical properties presented in Table 3 and support a limitation of the degradation due to the MAPP. Regarding G_{IIC} values, the

improvement of 240 % previously reported between both unaged composites in Figure 8 was maintained after ageing. However, unlike all other results presented so far, Rr values of G_{IIC} do not demonstrate a protective action of MAPP.

Like for unaged samples, PP-BL and PP-MAPP-BL composites behavior under DCB solicitation was found to be different. On the one hand, the fracture propagation in PP-BL composite takes place at the interface between both components and the average G_{IC} value is logically decreased from 171 to 96 J/m^2 due to the ageing in water. On the other hand, for PP-MAPP-BL, a shifting of the crack location from the interface to the bulk of BL was noticed like for unaged composites. Thus, the value of G_{IC} reported for PP-MAPP-BL characterizes the interfacial toughness of BL rather than the interface with PP. According to both ILSS and G_{IIC} Rr calculated for PP-MAPP-BL, it is possible to conclude that the value of the G_{IC} of the MAPP-BL/PP interface decreases but remains higher than that of BL even after ageing (i.e., 187 MPa). In addition, it is noteworthy that the Rr of 96 % tends to support the absence of degradation of BL presented in Table 2.

The fractography of aged composites is presented in Figure 10. No noticeable modification of the interface was induced by the accelerated ageing in water. The higher mechanical properties of PP-MAPP-BL after ageing are related to the remaining strong affinity between the components due to the MAPP coating. Conversely, PP-BL composites exhibit a dramatic lack of adhesion at the interface, which was also reported for unaged samples.

All in all, ageing in water induces a noticeable degradation of both composites' properties that could mainly be attributed to the interface degradation as suggested by Table 2 through 4. The improvement of the mechanical properties was maintained after ageing, and the degradation of the interface was restrained by the MAPP coating.

Table 3. Flexural properties and Rr of PP-BL and PP-MAPP-BL after a 400 hrs ageing in water

In MPa	PP-BL		Rr	PP-MAPP-BL		Rr
	Unaged	Aged		Unaged	Aged	
E$_f$(20 $^{\circ}$C)	5720±757	4050±925	71 %	7630±1200	6820±1220	89 %
UFS (20 $^{\circ}$C)	97.8±4.2	72.4±9.1	74 %	141±14.8	103±16.7	73 %
E' (25°C)	2747±682	2161±105	79 %	3640±48	3086±328	85 %
E' (100°C)	1570±473	887±92	56 %	2146±99	1452±199	68 %

Table 4. Interfacial properties and Rr of PP-BL and PP-MAPP-BL after 400 hrs ageing in water

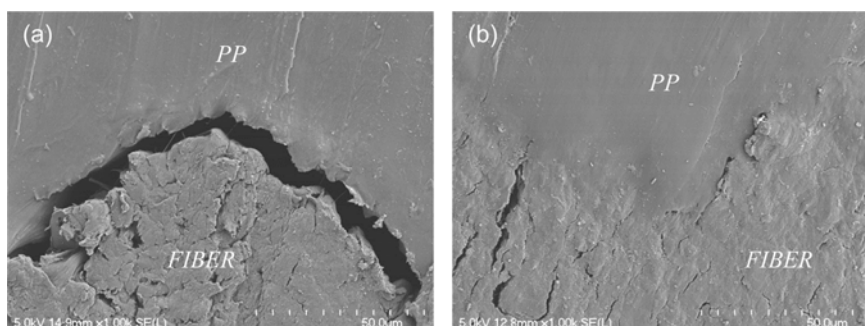| In MPa	PP-BL		Rr	PP-MAPP-BL		Rr
	Unaged	Aged		Unaged	Aged	
ILSS	6.4±0.5	4.0±0.4	63 %	16.6±1	12.8±0.7	77 %
G_{IIc}	175.8±49.3	90.2±24.0	51 %	598.2±86	294.9±35.4	49 %
G_{Ic}	171.3±17	95.9±40.4	56 %	195.7±23.9	187,2±35.4	96 %*

*Bamboo lamellae failure.

Figure 10. SEM micrographs of the interface between PP and BL after ageing; (a) without MAPP treatment and (b) with MAPP treatment.

Conclusion

Bamboo lamellae were successfully used and characterized to produce laminated composites which were fully studied regarding mechanical and interfacial properties. Thanks to the homogenous interfaces between PP and bamboo, uncommon normalized characterization methods such as end-notched flexure or double cantilever beam tests were successfully applied to characterize the interface properties and the effect of surface treatment (MAPP). The characterization methods have led to a quantification of the improvement of the interfacial fracture toughness in a mode I and II fracture opening. The evolution of the properties was also characterized after accelerated ageing in water. According to the results presented in this study, the following conclusions can be drawn:

1. Results of end-notched flexure and short beam shear tests converge and demonstrate that the MAPP coating leads to a great improvement in the ILSS and G_{IIC} of 240 and 160 % respectively.
2. Due to weak internal bonding in BL, G_{IC} of PP-MAPP-BL composites was not measurable with the DCB method. Still, DCB tests have proved that the enhancement of the opening mode I interfacial fracture toughness of composites is strongly limited by the bamboo-intrinsic G_{IC}. Thus, surface treatments appear not to be relevant to improve the fracture toughness in mode I as the improvement is quickly limited by the properties of BL.
3. Tests performed after accelerated ageing in hot water suggest that MAPP can limit the deterioration of the interface as retention rates of mechanical properties and, to some extent, interfacial properties were significantly higher in the PP-MAPP-BL composite.

The uncommon techniques employed in this study could provide a method for directly judging the effectiveness of surface treatments as well as their relevance and so the possibilities of natural fiber reinforced polymers.

Acknowledgments

References

1. J. Holbery and D. Houston, *JOM*, **58**, 80 (2006).
2. H. M. Akil, M. F. Omar, A. A. M. Mazuki, S. Safiee, Z. A. M. Ishak, and A. Abu Bakar, *Mater. Des.*, **32**, 4107 (2011).
3. G. Koronis, A. Silva, and M. Fontul, *Compos. Part B Eng.*, **44**, 120 (2013).
4. A. Khandual and S. Sahu in "Sustain. Fibres Fash. Ind." (S. S. Muthu and M. Gardetti Eds.), Vol. 2, pp.45-60, Springer Singapore, Singapore, 2016.
5. A. Célino, S. Fréour, F. Jacquemin, and P. Casari, *Front. Chem.*, **1**, 43 (2014).
6. M. S. Fogorasi and I. Barbu, *IOP Conf. Ser. Mater. Sci. Eng.*, **252**, 012044 (2017).
7. J. Gassan and A. K. Bledzki, *Appl. Compos. Mater.*, **7**, 373 (2000).
8. A. Arbelaiz, B. Fernández, J. A. Ramos, A. Retegi, R. Llano-Ponte, and I. Mondragon, *Compos. Sci. Technol.*, **65**, 1582 (2005).
9. H. Dhakal, Z. Zhang, and M. Richardson, *Compos. Sci. Technol.*, **67**, 1674 (2006).
10. A. Chilali, M. Assarar, W. Zouari, H. Kebir, and R. Ayad, *Compos. Struct.*, **206**, 177 (2018).
11. G. Cantero, A. Arbelaiz, R. Llano-Ponte, and I. Mondragon, *Compos. Sci. Technol.*, **63**, 1247 (2003).
12. X. Li, L. G. Tabil, and S. Panigrahi, *J. Polym. Environ.*, **15**, 25 (2007).
13. E. Zini and M. Scandola, *Polym. Compos.*, **32**, 1905 (2011).
14. A. Orue, A. Jauregi, U. Unsuain, J. Labidi, A. Eceiza, and A. Arbelaiz, *Compos. Part Appl. Sci. Manuf.*, **84**, 186 (2016).
15. T. P. T. Tran, J.-C. Bénézet, and A. Bergeret, *Ind. Crops Prod.*, **58**, 111 (2014).
16. Y. Xie, C. A. S. Hill, Z. Xiao, H. Militz, and C. Mai, *Compos. Part Appl. Sci. Manuf.*, **41**, 806 (2010).

17. S. Kalia, B. S. Kaith, and I. Kaur, *Polym. Eng. Sci.*, **49**, 1253 (2009).

18. C. M. Chan, L.-J. Vandi, S. Pratt, P. Halley, D. Richardson, A. Werker, and B. Laycock, *J. Appl. Polym. Sci.*, **135**, 46828 (2018).

19. T. J. Keener, R. K. Stuart, and T. K. Brown, *Compos. Part Appl. Sci. Manuf.*, **35**, 357 (2004).

20. S. Kaewkuk, W. Sutapun, and K. Jarukumjorn, *Compos. Part B Eng.*, **45**, 544 (2013).

21. S. Mohanty, S. K. Nayak, S. K. Verma, and S. S. Tripathy, *J. Reinf. Plast. Compos.*, **23**, 625 (2004).

22. C. K. Hong, N. Kim, S. L. Kang, C. Nah, Y.-S. Lee, B.-H. Cho, and J.-H. Ahn, *Plast. Rubber Compos.*, **37**, 325 (2008).

23. L. Osorio, E. Trujillo, A. W. Van Vuure, and I. Verpoest, *J. Reinf. Plast. Compos.*, **30**, 396 (2011).

24. P. Zakikhani, R. Zahari, M. T. H. Sultan, and D. L. Majid, *Mater. Des.*, **63**, 820 (2014).

25. K. M. M. Rao and K. M. Rao, *Compos. Struct.*, **77**, 288 (2007).

26. H. Wu, X. Li, F. Xiang, T. Huang, Y. Shi, and Y. Wang, *Chin. J. Polym. Sci.*, **30**, 199 (2012).

27. R. H. Boyd, *Polymer*, **26**, 323 (1985).

28. S. C. Lakkad and J. M. Patel, *Fibre Sci. Technol.*, **14**, 319 (1981).

29. D. W. Green, J. E. Winandy, and D. E. Kretschmann, "Wood Handb.-Wood Eng. Mater.", USDA Forest Service, Forest Products Laboratory, Madison, Wisconsin, 1999.

30. A. Bergander and L. Salmén, *J. Mater. Sci.*, **37**, 151 (2002).